

Chapter 2

Compact toroid magnetic field geometry, experiment and theory

Let us now examine the basic constraints imposed on a self-confined magnetized plasma ring that exists within in a cylindrically symmetric conducting vessel. The coaxial geometry of CTIX will require that we apply the following boundary conditions at both the inner and outer walls. It is natural to work in a cylindrical coordinate system (r, θ, z) .

The time varying part of the magnetic field \mathbf{B} of the compact toroid must satisfy the boundary conditions

$$\mathbf{n} \cdot \mathbf{B} = 0 \quad \mathbf{n} \times \mathbf{B} = \mu_0 \mathbf{K} \quad (2.1)$$

where \mathbf{K} is the surface current density. To satisfy the first condition, B_r must vanish at the wall. From the second condition we see that B_z is nonzero if there is a surface current K_θ in the azimuthal direction, and B_θ is nonzero if there is a current K_z in the axial or z direction.

Thus measurements of B_z and B_θ at the wall as a function of axial position and time (z, t) will let us know the state of the magnetic field and the current density at the boundary of the plasma.

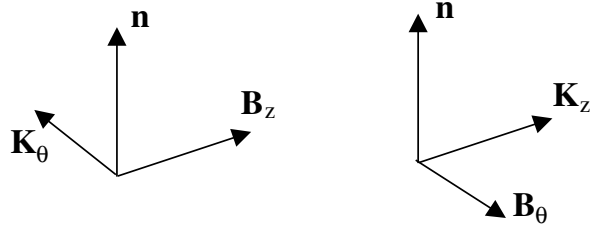


Figure 2.1: Relationship between surface current and magnetic field components

Much work has been done on the theory of force free equilibrium of plasmas in cylindrical, toroidal, and coaxial geometries. The relaxation of a magnetized plasma to a state of minimum magnetic energy, while global helicity is preserved, results in the Woltjer-Taylor force free equilibrium ($\mathbf{j} \times \mathbf{B} = \nabla P = 0$) given by

$$\nabla \times \mathbf{B} = \lambda \mathbf{B} \quad (2.2)$$

where $\lambda = \mu_0 j / B$.

Within a conducting vessel of coaxial geometry, and with the added assumption of zero axial surface current, $K_z = 0$, an axisymmetric solution exists that is separable and is expressible in terms of Bessel functions according to

$$B_r = B_0 \frac{k_z}{\lambda} \cos [k_z(z - z_0)] [J_1(k_r r) + f Y_1(k_r r)] \quad (2.3)$$

$$B_z = -B_0 \frac{k_r}{\lambda} \sin [k_z(z - z_0)] [J_0(k_r r) + f Y_0(k_r r)] \quad (2.4)$$

$$B_\theta = -B_0 \sin [k_z(z - z_0)] [J_1(k_r r) + f Y_1(k_r r)] \quad (2.5)$$

where $k_r^2 + k_z^2 \equiv \lambda^2$ relates the radial and axial wavenumbers to the magnetic eigenvalue λ .

To match the first boundary condition, values of k_r and f must be found such that $B_r(r, z) = 0$ at the inner and outer walls, $r = r_1$ and $r = r_2$ respectively. The radial term is

zero when

$$f = -J_1(k_r r_1)/Y_1(k_r r_1) = -J_1(k_r r_2)/Y_1(k_r r_2)$$

and so k_r must satisfy

$$J_1(k_r r_1)Y_1(k_r r_2) - J_1(k_r r_2)Y_1(k_r r_1) = 0$$

For the CTIX vessel, $r_1 = 3.34 \text{ cm}$ and $r_2 = 7.62 \text{ cm}$ in the acceleration section and so $k_r = 75.18 \text{ m}^{-1}$.

In order for $B_z = 0$ at $z = z_0$ and $z = z_0 + \Delta z$, $k_z = m\pi/\Delta z$. The axial extent of the compact toroid within CTIX tends to be about $\Delta z = 1$ meter and should be dominated by $m = 1$ mode, which implies that $k_z = 3 \text{ m}^{-1}$.

Using these values the Taylor state eigenvalue should be $\lambda = 75.24 \text{ m}^{-1}$. From this result we would also conclude that the ratio of the current density to magnetic field is

$$j/B = \lambda/\mu_0 = 5.98 \times 10^7 \text{ H}$$

where $H = 1 \text{ Henry} = C^2/kg \text{ m}^2$.

This means that for a modest CT surface field of 0.1 Tesla we would have a current density of about $6 \times 10^6 \text{ Amps/m}^2$ or 60 kA/cm^2 . This is roughly in agreement with measured currents.

One paper on this general topic is a 1993 paper discussing the Marauder plasma accelerator and their experiments [ref]. Their paper tackles the issue of MHD equilibrium for compact toroids, and presents a combination of analytical results, simulation and experimental results. Overall it is a very useful review of many relevant topics, and is the only published account I have been able to find that gives an analytic solution of $\nabla \times \mathbf{B} = \lambda \mathbf{B}$ in a coaxial geometry.

Despite their thoroughness, they made a few problematic mistakes in their presentation of the theory of force-free equilibria that are worth notice. The least of the errors was a simple typo, they gave the magnetic helicity as $\mathbf{A} \times \mathbf{B}$, when it should be $\mathbf{A} \cdot \mathbf{B}$ ¹.

¹See Appendix A for a discussion of Helicity of a force-free state

In the same section they made a more confounding mistake by writing down a believable-looking yet incorrect solution for the magnetic field of a force-free state $\nabla \times \mathbf{B} = \lambda \mathbf{B}$ in a coaxial geometry. Lastly, they listed a key reference that seemingly does not exist, even after much effort investigating a very wide margin of possibility for typographic or factual error.

As it relates to my present discussion, relying on the correctness of their published formulas caused some difficulty when I first attempted to make quantitative comparisons between theory and our experiment. The effect is that their formula gives a much larger B_z than B_θ inside the CT, whereas experiment showed that the two components are roughly equal (within a factor of 2). Their formula for B_z had a coefficient (k_r^2/k_z^2) , but when the curl is taken and field components are compared, I found that B_z should just depend on (k_r/k_z) , not squared. The corrected formulas listed above (2.3 - 2.5) actually satisfy $\nabla \times \mathbf{B} = \lambda \mathbf{B}$, while their counterparts in the 1993 paper did not. When this is corrected, the ratio of B_θ/B_z approaches unity within the CT, basically in agreement with experiments.

A further point of refinement can be made, which will be examined more closely in the next section, if the bending of the field lines near the probe port hole is taken into account. This bending results in an effective depth of the probe measurements that is approximately 0.5 cm into the interior of the plasma. The Taylor state model predicts that at this depth, the magnitude of B_θ should be very close to 1/2 of the value of B_z . More generally, it also predicts that within the CT the ratio B_θ/B_z should be only a function of radial position.

When compared to our experiments, this first prediction that our probes should measure $B_\theta = \frac{1}{2}B_z$ is right on the mark when looking at the time of the peak value of B_z at the center axial position of the CT. On the majority of shots we observe a noticeable dip in the B_θ signal that is coincident with the CT center, whose amplitude is very close to 1/2 the peak value of B_z . My interpretation is that this central dip in B_θ is due to Taylor state fields.

However, on almost every shot, the behavior of B_θ inside the CT disagrees qualitatively with the second prediction of the Taylor state model; that the ratio B_θ/B_z is not a function of z.

Our measurements show a significant ramping up of B_θ , going from zero at the leading edge of the CT to about 1/2 to 3/4 of the value of $B_z(t_{peak})$, by the time the back edge of the CT has passed the probe. Then when the probe crosses over into the pushing field, B_θ increases to be at or above the value of the peak of B_z .

This linear ramp-up of B_θ inside the CT is not accounted for by the Taylor state, and some kind of modification to the simple force-free state is required.

One physical complication that may account for the departure away from the simple Bessel function solution is the nature of the current paths near the wall. In the actual device, acceleration of the CT is accomplished by large rail-gun currents that flow axially down the inner conductor, then flow radially through the plasma, and return via the outer conductor.

Because magnetic field is frozen into the plasma during formation, large poloidal currents and toroidal magnetic fields persist in the CT as it propagates. In the outer regions of the CT poloidal currents that intersect the wall are able to penetrate into the conducting wall one skin depth and then flow axially through the walls some distance before merging back into the plasma.

Thus in the vicinity of the CT there is axial surface current $K_z \neq 0$ and so $B_\theta \neq 0$ at the walls in this region, in disagreement with one assumption that leads to the closed form solution (2.3 - 2.5). Also, where poloidal current enters or exits the wall $j_r \neq 0$ yet the boundary conditions require that $B_r = 0$ at the wall, in contrast to the force-free model that predicts a constant proportionality between all components of current density and magnetic field, $\mathbf{j} \times \mathbf{B} = 0 \longrightarrow \mathbf{j} = \frac{\lambda}{\mu_0} \mathbf{B} \longrightarrow j_r = \frac{\lambda}{\mu_0} B_r$ and so this is in contradiction with observation at least in the vicinity of the walls.

The observation that $j_r \neq 0$ at the walls is well supported by measurements of B_θ . We can evaluate Ampere's equation $\nabla \times \mathbf{B} = \mu_0 \mathbf{j}$ in cylindrical coordinates with assumed axisymmetry.

The resulting components of \mathbf{j} are:

$$j_r = -\frac{1}{\mu_0} \frac{\partial B_\theta}{\partial z} \quad (2.6)$$

$$j_\theta = \frac{1}{\mu_0} \left(\frac{\partial B_r}{\partial z} - \frac{\partial B_z}{\partial r} \right) \quad (2.7)$$

$$j_z = \frac{1}{\mu_0 r} \frac{\partial r B_\theta}{\partial r} \quad (2.8)$$

So we can find j_r at the outer wall by measuring the z dependence of B_θ with surface probes. We observe large radial currents j_r of $\sim kA/m^2$ entering and exiting the outer wall.

The interesting questions involve exactly how the CT magnetic geometry varies away from a true force-free Taylor equilibrium when the CT is strongly accelerated.

The surface magnetic field of CTIX plasma has been measured. The details of our methods will be discussed in the remaining sections of this chapter.

2.1 Hall term, $\mathbf{j} \times \mathbf{B}$

2.2 Magnetic field measurements

The measurements of the axial and toroidal magnetic field components are done with special magnetic probes, each component is measured with its own $1\text{ cm} \times 1\text{ cm}$ square loop coil of several turns. The two loops are wound at right angles to each other through small holes at the tip of a long plastic rod (see figure 2.2).

As the net magnetic flux through the loop changes when the magnetized plasma flows around it, a corresponding current is induced in the wire that is proportional to the time derivative of the instantaneous magnetic field at the loop. This current is put through a passive RF integrator that effectively takes the time integral of the signal, and the output signal is digitized.

This recorded signal has some further numerical corrections applied to it in order to compensate for an inherent droop effect of the integrator circuit. The final product is a well calibrated measure of the magnetic field strength as a function of time at the position of the loop.

Some complications arise when we attempt to compare the experimentally measured magnetic field with the predictions of analytic or computational models. The non-experimental models presently do not take into account some important details of the actual vessel geometry in the vicinity of the magnetic field probe ports.

Each magnetic probe port consists of a 0.874 inch hole in the stainless steel outer conductor, with a stainless tube (0.874 inch inner diameter) welded to the hole and extending radially outward (about 1 inch) to a flange that makes an o-ring vacuum seal with a 1/2 inch diameter ceramic tube. The ceramic tube is 6 inches long with one closed end that is inserted into the vessel so that the tip of the ceramic tube is approximately flush with the inner surface of the outer conductor. The other end of the ceramic tube is open to the air, and a plastic rod with the magnetic probe coils at its end is then inserted fully into ceramic tube so that the coils are as close to the plasma as possible.

The ceramic tube acts in three ways: 1) as high voltage insulator to protect the probe coils from the ~ 10 kV potential of the outer conductor, 2) as a vacuum seal and vessel wall that separates the atmospheric pressure from the 10^{-6} Torr vacuum inside CTIX, 3) and as dielectric boundary that lets magnetic field at the edge of the plasma to enter the probe coil and be detected.

Thus the probe coils are actually inside a finite-sized conducting cylindrical well, approximately 0.874 inches in diameter and 0.765 inches deep. The boundary conditions are significantly different than if the port was not there. As the magnetized plasma flows by a port, it dips into the annular gap between the outside of the ceramic tube and the inside of the stainless steel. Even if plasma flow effects are ignored, the edge magnetic field will expand to fill the conducting well of the port and there will be a gradient in the field as components change to match the boundary conditions. So the result of the measurement depends strongly on the precise depth of the probe position inside the port well.

One key characterization that is needed to properly interpret the magnetic measurements is to calculate an effective depth of the experimental magnetic measurements. The idea is that because of the well geometry of the port, the probes are effectively measuring the fields at some point in the

interior of the plasma, some small but not exactly zero distance away from the outer wall.

This would help reconcile the fact that the analytic Bessel function solution to the Woltjer-Taylor force free equation has zero B_θ at the walls, while our probe measurements show it to be non-zero. If we accept that the probe is not actually measuring exactly “at the wall” but rather at the effective depth into the interior, then the question of consistency is relaxed. The comparison between model and experiment would then become a quantitative comparison of the ratio of field components at the effective depth.

A reasonable approximation can be made by considering the magnetostatic problem with an ideal conductor in the shape of the magnetic probe port. This ignores any plasma dynamics that might effect the measurement, but in the case of a low beta plasma, like our CT, the magnetic field is boss. And although we consider a magnetostatic problem, this isn’t such a bad approximation given that the relevant MHD transit timescales are many orders of magnitude slower than the speed-of-light transit timescale for the probe port system. Still, we hope to greatly improve upon these preliminary estimates in the future, and in part, I am documenting the details of my work here in

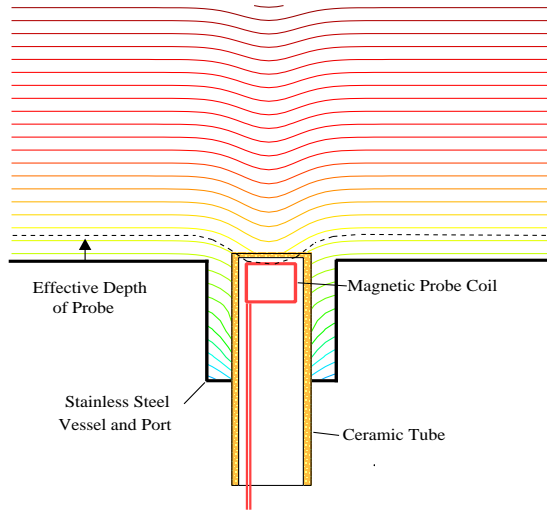


Figure 2.2: Sketch of magnetic probe port and the effect it would have on a uniform field

order to provide a starting point for future work, including some 3-D MHD simulations proposed for the near future.

We want to find the geometric effect on field lines near the port, given that the field is uniform at infinity. There would be some field line that intersects the tip of the probe coil. If we follow this field line away from the port sufficiently far, it will level off uniformly. The effective depth of the probe would then be defined as the distance from the wall of this field line when it is far from the port. Additional calibration factors due to field expansion must also be taken into account. The effect is that the measured field is very strongly dependent on the exact radial position of the probes. The interior fields of the CT are several times larger than what we would expect without these additional calibration factors. During the previous calibration of our probes these field expansion effects should have been implicitly taken into account via the method that was used. After several theoretical considerations have been made will compare predicted and measured calibration factors.

To tackle these issues we can consider a variety of approaches. The simplest is to regard the probe well as simply a hole in the vessel wall which we can reasonably approximate as flat. The magnetostatic field near a circular hole in a thin flat conducting plate has a tractable analytic solution expressible as an integral that can be numerically evaluated. [ref jackson] The magnetic field \mathbf{H} has the form $\mathbf{H} = -\nabla\phi_M$ where the magnetostatic potential ϕ_M is given by

$$\phi_M = \begin{cases} -H_0y + \Phi^1(\vec{x}) & \text{if } z > 0 \\ -\Phi^1(\vec{x}) & \text{if } z < 0 \end{cases}$$

This form guarantees that $\mathbf{H} = -\nabla\phi_M$ will approach a constant vector of magnitude H_0 in the y-direction, as you move away from the hole in the upper half space, while the field goes to zero in the lower half plane. Thus, $\Phi^1(\vec{x})$ describes the localized variation away from complete uniformity.

The solution of $\nabla^2 \Phi^1 = 0$ given the boundary conditions of a hole of radius a can be found by Bessel series expansion in cylindrical coordinates (ρ, ϕ, z)

$$\Phi^1(\vec{x}) = \frac{2H_0a^2}{pi} \int_0^\infty dk j_1(ka) e^{-k|z|} J_1(k\rho) \sin \phi \quad (2.9)$$

where $j_1(x) = \frac{\sin x}{x^2} - \frac{\cos x}{x}$ is the spherical Bessel function of order 1, and $J_1(x)$ is just an ordinary Bessel function of the first kind, order 1.

This solution is attractive to work with because it is fully 3-dimensional, so the total flux through a coil oriented arbitrarily in space can be accurately calculated. However, the simplicity of the boundary geometry yields some quantitatively different effects than the actual, more complex, probe well geometry. The root cause of this discrepancy is that in the case of the simple hole, the field is allowed to expand out infinitely into the void beneath the plane, instead of just the finite sized well that we actually have. This means that more total flux enters the hole than would enter the opening of a well. Since more flux enters, the field beneath the plane is stronger for the hole geometry than the well, i.e. the field below the hole is diminished less than it would be inside the well. Then the calibration factor $\frac{H_0}{\langle H \rangle_p}$ due to field diminishment caused by expansion, would be somewhat less in the hole geometry than for a finite well.

Secondly, each field line that enters the hole will go deeper than it will in the case of a finite well. Thus for a given probe position, the resulting effective depth will be noticeably larger for the simple hole than it would be for the finite well.

Since we are primarily seeking an accurate estimate of the effective depth of the probe in order to compare measured field components to those predicted by theory, we need to do a better job at including the effects of the finite well geometry. So, let us consider a few more possible ways to approach the full magnetostatic problem for a finite well.

The most ambitious route would be to perform a similar Bessel series expansion of the potential as above, but with the added complication that two distinct regions would need to be analyzed separately, then a unique solution could be found to the full problem by matching series

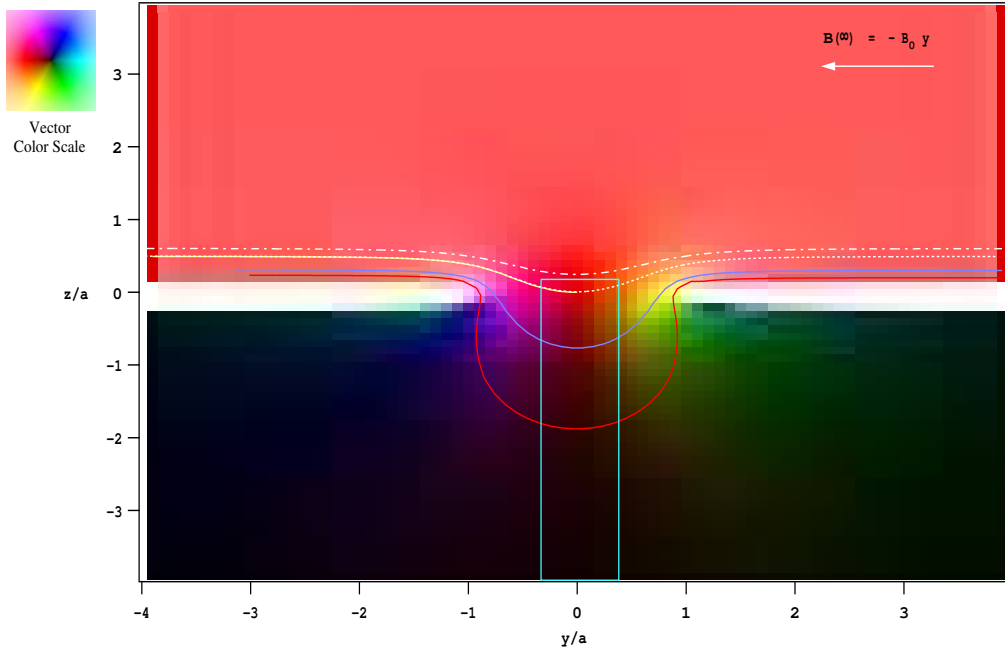


Figure 2.3: Analytic result for magnetic field near a hole in a conducting plane. Here the field vectors are represented by a color-wheel type coloring of the complex plane, which corresponds to the (y, z) directions in physical space. Red indicates a vector pointing directly in the $-y$ direction, while other colors represent vectors at other directions as indicated by the color legend in top left. Vector magnitude is represented by a color's brightness, with black for the zero vector. This color code avoids the “pick-up-stix” effect that can occur with arrow-field representations. A sampling of field lines are also plotted to guide the eye.

coefficients at the interface of the two regions.

The natural choice would be to set one region as the cylindrical volume inside the well, with conducting boundary conditions on the side and base, and the interface matching condition on the top surface. Then the second region would be the upper half space above the plane, with conducting boundary at the $z = 0$ plane, everywhere except for the circular disk where the field needs to match the other region. To implement this, first some analytic simplifications to the general Bessel series would need to be made that take into account the different symmetries of the two regions. Then you would try to see how matching the coefficient at the interface would constrain the form of the solution. However, at this point, progress toward a purely analytic solution begins to fall into that grey unknown between difficult and impossible, and a numerical solution of the system

of coupled integral Fourier-Bessel equations becomes the only tractable option. Then considering that the primary aim of my work was not to spend weeks or months to perfectly solve an advanced 3-D magnetostatic problem by numerical evaluation of Fourier-Bessel equations, I decided to find a simpler, quicker approach.

Since the diameter of the probe coil is relatively small compared with the diameter of the port hole, a 2-D approximation can be made that should be quite accurate for the fields near the central plane of the probe port well. Field expansion effects should be more faithfully recreated by a 2-D solution of the right cross-section geometry than a 3-D solution of the wrong cross-section geometry.

Essentially, the problem in 2-D is equivalent to a field above a conducting plate with an infinitely long trench cut into it, with a rectangular cross-section. If the trench runs in the x-direction, then the solution of the field will be independent of x, it will only vary in the 2-D (y,z) plane. This 2-D solution would correspond to the $x = 0$ plane in the full 3-D problem.

One standard analytic method for dealing with this 2-D problem is the use of conformal mapping. [smythe][F.M. Henderson, Elliptic functions with complex arguments, Univ. Michigan Press 1960, pg 10]. In general it is possible to transform the upper half of the complex plane into the interior of a polygon, by a conformal map according to a straight-forward formula.

For the case at hand, the resulting polygon would be the “upside-down top hat” shape of the vacuum-conductor boundary. It would have four vertices, and interior angles of $\{\frac{3\pi}{2}, \frac{\pi}{2}, \frac{\pi}{2}, \frac{3\pi}{2}\}$. The original untransformed plane is the z-plane, and the transformed plane is the w-plane; the mapping function is $w = w(z)$, which is formulated implicitly through a differential relation:

$$\frac{dw}{dz} = G \frac{(z - c)^{\frac{1}{2}}(z + c)^{\frac{1}{2}}}{(z - 1)^{\frac{1}{2}}(z + 1)^{\frac{1}{2}}} = G \sqrt{\frac{z^2 - c^2}{z^2 - 1}} \quad (2.10)$$

Here, G is a complex constant that accounts for overall scale and orientation of the resulting polygon, and c is a positive real number, where the points $z = \pm c$ get mapped to the vertices at the opening of the well $w = \pm a + bi$, which are labeled points D and A, respectively (see Fig 5). To

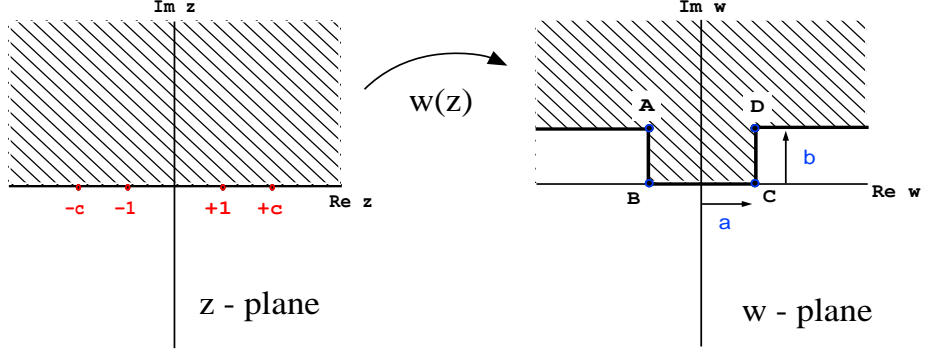


Figure 2.4: Conformal mapping method for 2-D approximation

solve for $w(z)$ we need to take the indefinite path integral, where the integration dummy variable u takes a path from $u = -\infty$ to $u = z$, which is route-independent as long as no branch cuts (along $\text{Im } z = 0$) are crossed. The integral is

$$w(z) = G \int_{-\infty}^z \sqrt{\frac{u^2 - c^2}{u^2 - 1}} du = Gc \int_{-\infty}^z \sqrt{\frac{1 - (\frac{u^2}{c^2})}{1 - u^2}} du \quad (2.11)$$

This integral is not possible to evaluate “analytically” in terms of elementary functions, and does not appear in any standard table of integrals. This is because it corresponds to a combination of elliptic integrals of the second kind, usually notated by $E(k, z)$, here taking a complex argument. Some progress can be made from this point,

$$w(z) = Gc[E(1/c, z) - E(1/c, \infty)] \quad (2.12)$$

and the resulting dimensions of the well radius = a , depth = b , are determined from G and c according to

$$a = Gc[E(1/c) - E(1/c, \infty)], \quad b = Gc[K(\sqrt{1 - (1/c)^2}) - E(\sqrt{1 - (1/c)^2})] \quad (2.13)$$

where $K(k)$ and $E(k)$ are complete elliptic integrals of the first and second kind, respectively. The

proportions of the well, ie the ratio b/a is then independent of G and has the form

$$\frac{b}{a} = \frac{K(\sqrt{1 - (1/c)^2}) - E(\sqrt{1 - (1/c)^2})}{E(1/c) - E(1/c, \infty)} \quad (2.14)$$

It was not too difficult to implement a direct numerical evaluation of the path integral (2.11), and some qualitatively good initial results were obtained.

Once you have the mathematical mechanics set up, it is very easy to find the shape of field lines in the vicinity of the well. You just sequentially evaluate $w_p = w(z_p)$ N times, where $z_p = (x_0 + p \cdot \Delta x) + iy$ for point index taking values of $p \in \{0, 1, 2, \dots, N\}$. This just maps the horizontal line $\text{Im } z = y = \text{constant}$ to the corresponding field line. The resulting array of complex numbers w_p can be plotted to visualize the field line in space.

Furthermore, the effective depth can be found by tracking field lines away from the well and then finding how high above the wall they are after going several hole-radii away from the well. Field expansion ratios can be calculated by comparing the distance between two neighboring field lines, when they are far from the well, vs when they are at the center of the well.

Since the magnitude of the magnetic field is proportional to the density of flux lines, in this way we can get the ratio of the far field to its corresponding value of the distorted near field. To measure the average flux through the probe coil, we just choose one field line that passes through the upper tip of the coil, and a second that passes through the lower tip of the coil. If the distance between these two field lines far from the probe well is δz and the height of the probe coil is Δz_{coil} then the calibration factor due to field expansion is $C_{exp} = \frac{\Delta z_{coil}}{\delta z}$.

The one stumbling block that prevented the full application of this method to solve the problem at hand, is that for reasons not yet understood, the ratio of b/a was not precisely controllable with the algorithms I have implemented. Essentially, only a single value of $b/a \sim 1$ was achievable, regardless of the choice of c and G . An intrinsic part of the problem is that my algorithm was divergent for points close to the real axis in the z -plane. This prevented me from making an accurate determination of what the real b/a ratio was for any particular instance of the mapping. There is

some hope that after some further work with elliptic integrals, the increased insight and experience may lead to a resolution of the bugs in my code. But for the sake of time management, I abandoned this semi-analytic approach and switched to an even simpler fully numeric 2-D iterative relaxation method.

We begin this final (successful) approach with a significant practical simplification. The magnetic field vectors themselves are not really important to find the effective depth and expansion factor, especially if we are only considering a 2-D case. Really we just need to know the shape of the flux surfaces on which the magnetic field lines reside. The simplifications arises from the fact that the magnetostatic potential ϕ_M is what we call the *harmonic dual* of the electrostatic potential ϕ_E .

The concept of harmonic duality is that if two scalar functions satisfy the Laplace equation ($\nabla^2 \phi = 0$, which is the definition of harmonic here) on the same boundary geometry, we say that the functions are dual to each other if one function satisfies Dirichlet boundary conditions ($\phi_1 = \text{constant}$), while the second function satisfies Neumann boundary conditions ($\frac{\partial \phi_2}{\partial n} = \text{constant}$). The result is that equipotential surfaces of ϕ_1 correspond to flux surfaces of ϕ_2 , and vice versa. This is due in part to the fact that equipotential surfaces and the flux surfaces for the same potential function are locally orthogonal to each other. To go from a potential function to its harmonic dual, we just have to interchange the role of equipotentials and flux surfaces, and the resulting potential will still satisfy the Laplace equation, but with the dual boundary condition.

The magnetostatic potential satisfies the Neumann boundary condition at the surface of the conductor, while the electrostatic potential for the same conductor geometry satisfies the Dirichlet boundary condition. Therefore we can find the flux surfaces of the magnetic field by actually computing the equipotential surfaces of the dual electrostatic potential problem. This is an advantage because Dirchelet boundary conditions are intrinsically simpler in that you don't have to evaluate derivatives to apply them, and they lend themselves to numerical solution by iterative relaxation methods.

I have implement a simple Gauss-Seidel method using a 2-step iteration on two interleaved

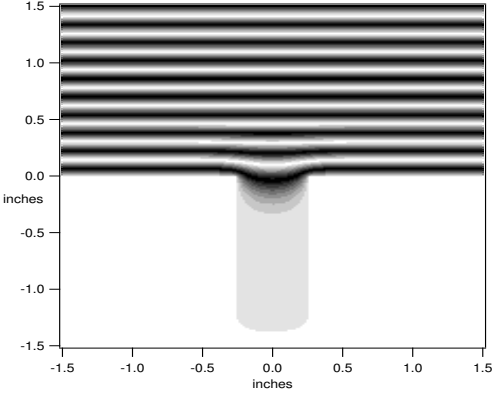


Figure 2.5: 2-D Relaxation simulation result of magnetic field near a conducting port well

square meshes. [ref jackson 1.13 pg 47-50] (see Appendix B for details)

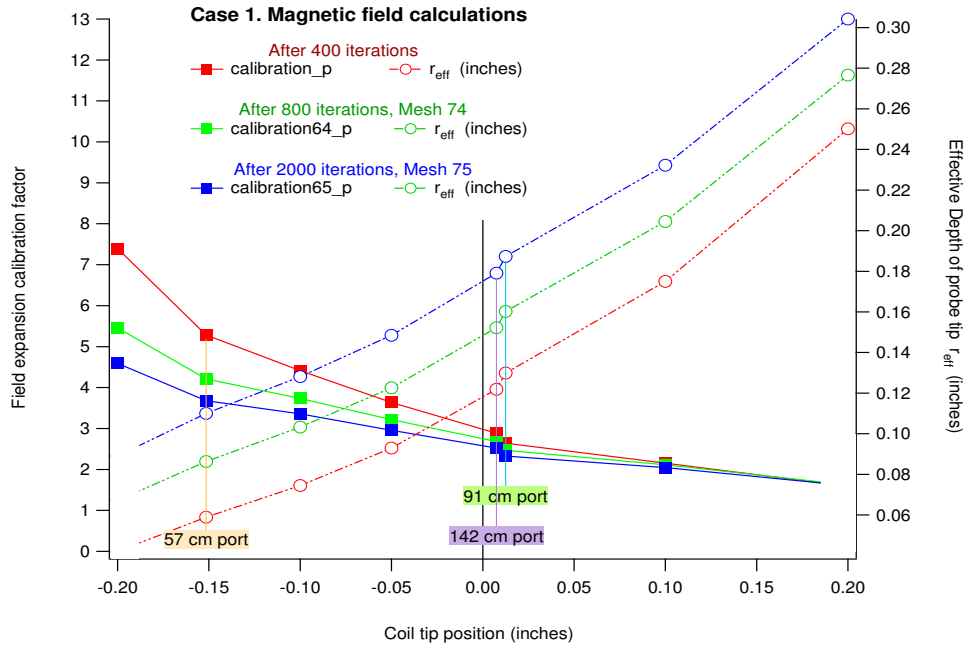


Figure 2.6: Probe position dependent trends in the expansion factor (left) and the effective depth of measurement (right) for magnetic field expansion into full volume of well. Position zero corresponds to the probe coil tip being flush with the inner edge of the port hole.

We also have an independent consideration that leads to similar relative calibration between the primary set of magnetic probes. There is good reason to expect that toward the end of the

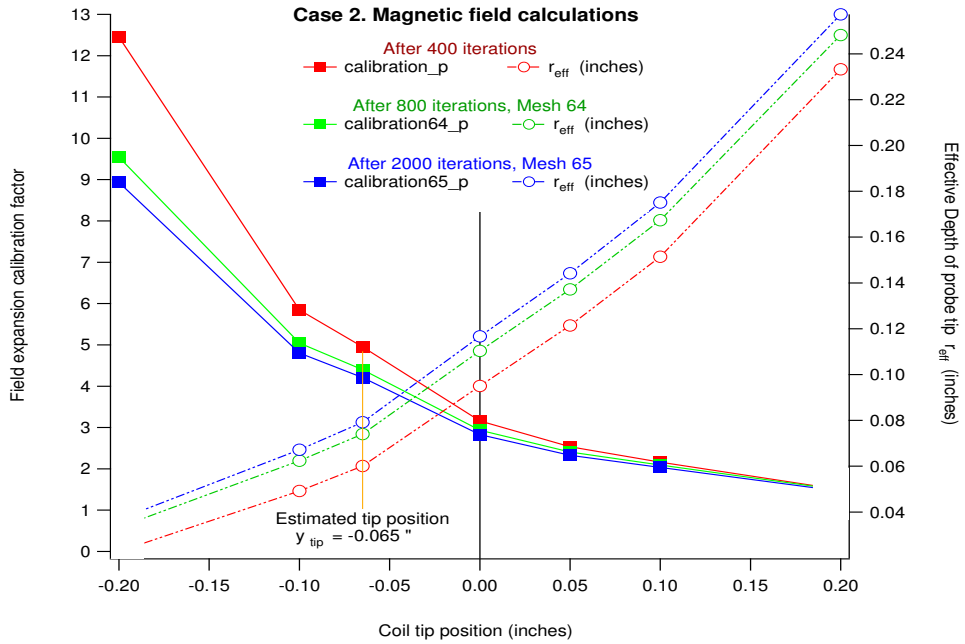


Figure 2.7: Probe position dependent trends in expansion factor (left) and effective depth of measurement (right) for magnetic field expansion into only partial volume of well due to field exclusion by stagnant plasma. Position zero corresponds to the outer surface of the ceramic probe sleeve.

acceleration process the B_θ pushing fields behind the CT should have mostly come to an equilibrium state that is nearly uniform as a function of z . When we look at the actual B_θ data we see a systematic discrepancy between the measurements at the three locations that could either mean a highly reproducible non-uniformity of $B_\theta(z, t)$ that depends on z in an exactly fixed way, or that previous calibration factors for the probes were slightly off by differing amounts. The effect of probe depth in a conducting well of the probe port provides the simplest explanation for this error, and it should be corrected for.

2.3 Lagrangian interpolation of probe signals

Report specific results relevant to magnetic geometry, details of algorithm are left for the appendix. *Analysis finished, but not written yet.*

2.4 Characterization of CT modes

show standard “typical” mode and a variety of non-typical modes show time signals and reconstructed axial dependence at various times

2.5 Comparison between experiment, theory, and simulation

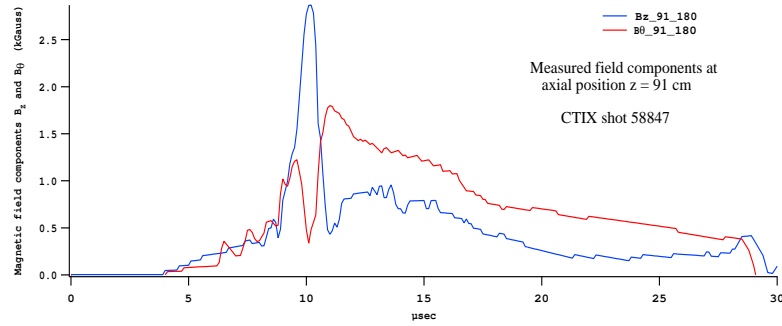


Figure 2.8: Measured magnetic fields at $z = 91$ cm

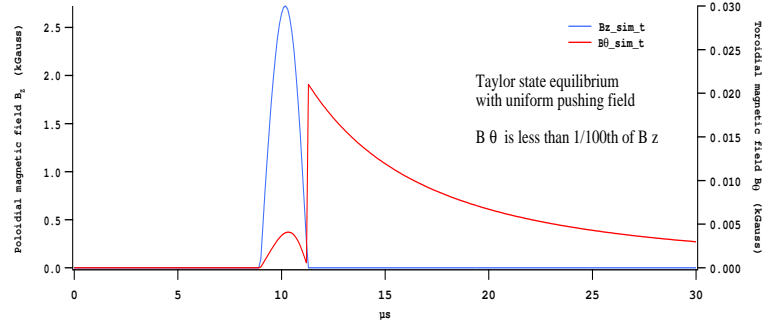


Figure 2.9: Accelerated Taylor equilibrium with axial compression (absolute value of B_θ)

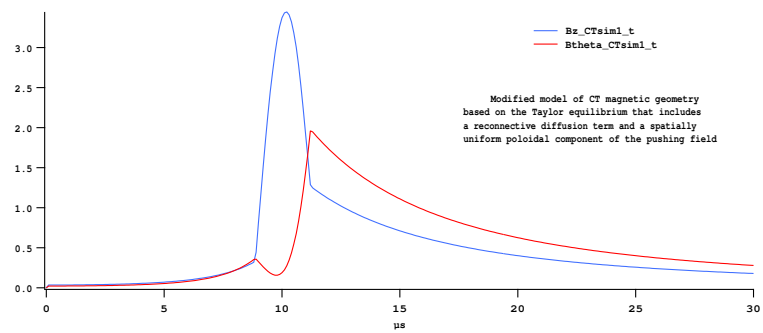


Figure 2.10: Accelerated Taylor-like equilibrium model that is not at an energy minimum, and includes compression and a reconnective diffusion term